NGU REPORT 2024.036

Helicopter-borne magnetic, electro-magnetic and radiometric geophysical survey in a selected area of Møre og Romsdal County.

GEOLOGY FOR SOCIETY
SINCE 1858

GEOLOGICAL SURVEY OF NORWAY
- NGU -

NGU REPORT 2024.036

Helicopter-borne magnetic, electro-magnetic and radiometric geophysical survey in a selected area of Møre og Romsdal County.

GEOLOGICAL SURVEY OF NORWAY
- NGU -

NGU REPORT

Geology for society

Geological Survey of Norway
P.O. Box 6315 Torgarden
NO-7491 Trondheim, Norway
Tel. +47 73 90 40 00

Report no.: 2024.036
ISSN: 0800-3416 (print)
ISSN:2387-3515 (digital)
Grading: open

Title: Helicopter-borne magnetic, electro-magnetic and radiometric geophysical survey in a selected area of Møre og Romsdal County.

Authors: Frode Ofstad, Tom Kristiansen, Giorgios Tassis, Frida Mathayo Mrope, Håvard Thorsnes, Emily Rose Norum and Marie-Andrée Dumais.
Client: NGU
County: Møre og Romsdal
Municipalities: Molde, Ålesund, Kristiansund, Hustadvika, Tingvoll

Map-sheet name (M=1:250.000):
Map-sheet name (M=1:50.000): 1220:1-3, 1320:1-4, 1321:2-3
Area name and grid-reference: Molde, WGS84 UTM32N 410000E, 6960000N
Numbers of pages: 30
Price (NOK): 120

Map enclosures:
Fieldwork carried out: June 20th, 2022, to October 2nd, 2024.
Date of report: December 2024
Project no.: 388901
Person responsible: Marco Brönner
Keywords: Airborne, geophysics, magnetic, gamma-ray spectrometry, electromagnetic, technical report

Summary:
NGU conducted an airborne geophysical survey in a selected area of Møre og Romsdal County, covering parts of Kristiansund, Averøy, Hustadvika, Aukra, Gjemnes, Tingvoll, Rauma, Vestnes, Molde and Ålesund municipalities, as a cooperation between Møre og Romsdal county, and NGU, as part of NGU's general airborne mapping program. The data acquisition in the Møre area was started in June 2022 and finally completed in October 2024.

This report describes and documents the acquisition, processing and visualization of the acquired datasets and presents them in maps. The geophysical surveys consist of 13,000 line-km data, covering an area of 2,600 km^2 flown from the base at Eide, Molde and Vestnes.

The NGU modified Geotech Ltd. Hummingbird frequency domain electromagnetic system supplemented by an optically pumped cesium magnetometer and the Radiation Solutions 1024 channels RSX-5 spectrometer mounted on a AS350-B3 helicopter were used for data acquisition. The data collected were processed at NGU, using Geosoft Oasis Montaj software. Raw total magnetic field data were corrected for diurnal variation and levelled using Geosoft micro-levelling algorithm. Radiometric data were processed using standard procedures as recommended by International Atomic Energy Association (IAEA). Electromagnetic data were filtered and levelled using both automated and manual levelling procedures. Apparent resistivities were calculated from in-phase and quadrature data for three coplanar frequencies (880 Hz, 6.6 kHz and 34 kHz), and for two coaxial frequencies (980 Hz and 7 kHz) separately using a homogeneous half-space model. All data were gridded using cell size of 50x50 meters and presented as 30% transparent grids on top of topographic maps.

Table of contents

1. INTRODUCTION

During the years 2022, 2023 and 2024, NGU acquired airborne geophysical data in Møre og Romsdal county. The helicopter survey presented in this report covers part of Kristiansund, Averøy, Hustadvika, Aukra, Gjemnes, Tingvoll, Rauma, Vestnes, Molde and Ålesund municipalities. The processed data amounts to 13,000 line-km, or 2,600 km^2, where the different area measured is shown in Figure 1.

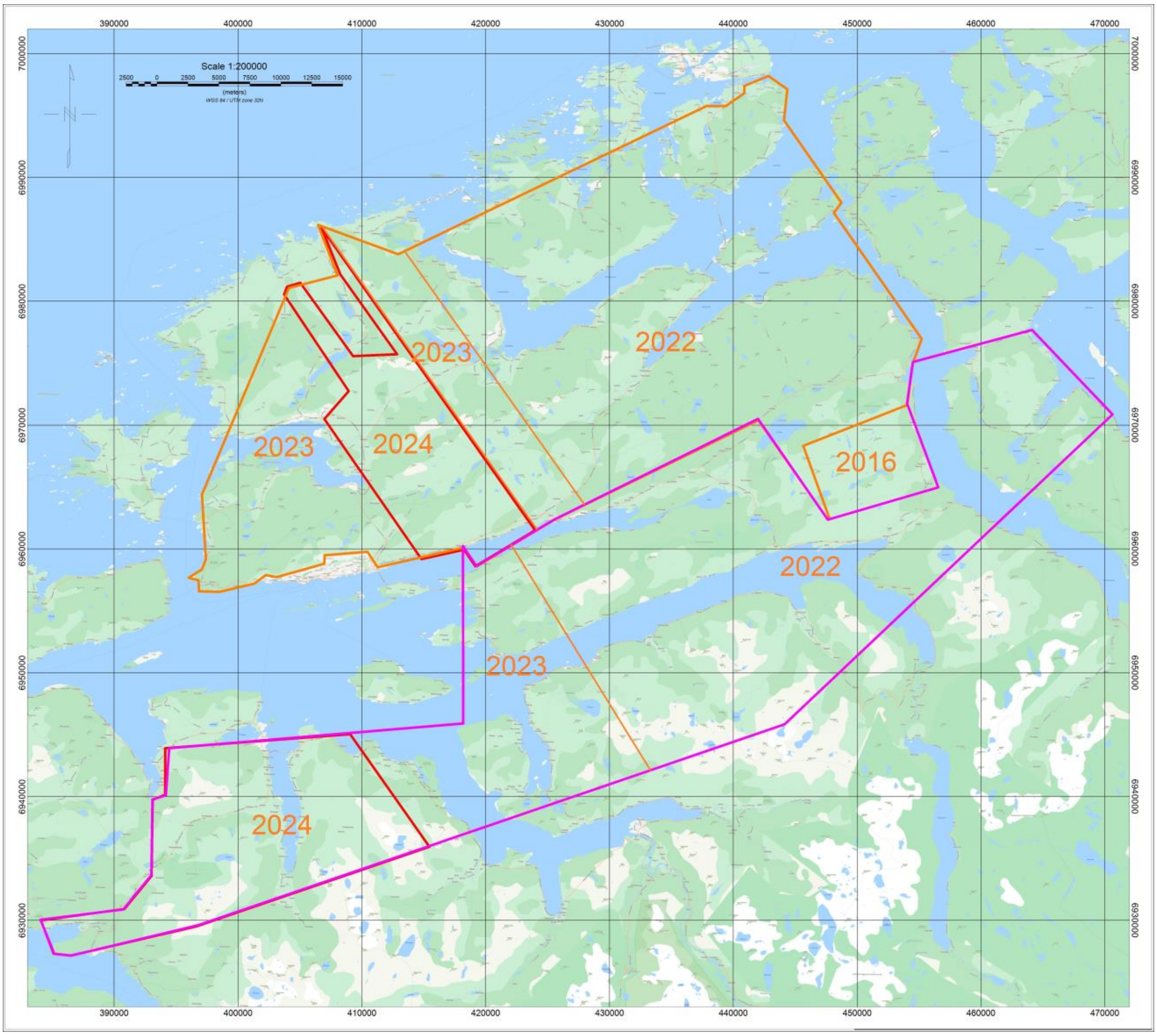

Figure 1: The helicopter survey area in Møre og Romsdal, with the year of survey indicated.

The objective of the airborne geophysical survey was to obtain a dense high-resolution magnetic, electromagnetic, and radiometric data set over the survey area. These data are required for the enhancement of a general understanding of the regional geology of the area, with adjoining area is covered by recent airborne surveys in Romsdalsfjorden (2015) and Raudsand (2016).

In this regard, the new data can be used to map contacts and structural features within the survey area. It also improves defining the potential of known zones of mineralization, their geological settings, and identifying new areas of interest, as the dataset fills a gap in the high-resolution geophysical surveys of the region.

The survey incorporated the use of a Hummingbird™ 5-frequency electromagnetic (EM) system supplemented by a high-sensitivity cesium magnetometer, gamma-ray spectrometer, and a helicopter mounted radar altimeter. A GPS navigation computer system with flight path indicators ensured accurate positioning of the geophysical data with respect to the World Geodetic System 1984 geodetic datum (WGS-84).

2. SURVEY SPECIFICATIONS

2.1 Airborne survey parameters

NGU used a modified Hummingbird™ EM and magnetic helicopter survey system designed to obtain low level, slow speed, detailed airborne EM, and magnetic data (Geotech 1997). The system was supplemented by a Radiation Solutions RSX-5, 1024 channel gamma-ray spectrometer, installed under the main body of the helicopter, used to map ground concentrations of uranium, thorium and potassium, and the total counts radiation.

The data were acquired in four parts with four different helicopters; first from June 20th to August 31st, 2022, from a base established at Eide, then continued from July 8th to August 6th, 2023, from a base at Tusten ski resort near Molde, then from May 29th to June 8th, 2024, again at Tusten, and finally completed between September 26th and October 2nd, 2024, from a base near Vestnes. Eurocopter AS350-B3's. First, LN-OSD, owned by Pegasus Helicopter AS was used in 2022, then LN-OSU from Pegasus in 2023. LN-OPN was used in the spring of 2024, the autumn flights done with LN-OGL, both from Airlift.

The survey lines were spaced 200 meters apart, with lines oriented at 145° in UTM zone 32. In average, the helicopter altitude was 86 meters above the ground when on survey line. The magnetic and electromagnetic sensors are housed in a single seven-meter-long bird, towed 30 meters below the helicopter, and flown at an average of 56 meters above the topographic surface. Flight survey specifications are shown in Table 1.

The Raudsand area, measured by NGU in autumn of 2016, using LN-OGL, was included in the dataset. This area was flown with 160° and we use only half the lines to match the surrounding dataset.

Table 1. Flight specifications

Survey name	Surveyed lines (km)	Surveyed area (km^2)	Line direction (°)	Line Separation (m)	Average speed (km/h)
More og Romsdal	13,000	2,600	145	200	69
Raudsand	350	70	160	200	85

The survey area covers the area between Kristiansund, Hustadvika, Molde, Tingvoll to Sjøholt. Rugged terrain and abrupt changes in topography affected the aircraft pilot's ability to 'drape' the terrain, meaning the average instrumental height was sometimes higher than the standard survey instrumental height, which is defined as 30 meters plus a height of obstacles (trees, power lines etc.) for EM and magnetic sensors.

During the survey line acquisition, the ground speed of the aircraft varied from 10 to 120 km/h depending on topography, wind direction and its magnitude. On average the ground speed during measurements is calculated to 69 km/h (19 m/s). Magnetic data were recorded at 0.2 second intervals resulting in approximately 3.8 meters average point spacing.

EM data were recorded at 0.1 second intervals resulting in data with a sample increment of 1.9 meters along the ground on average. Spectrometry data were recorded every 1 second giving a point spacing of approximately 19 meters. The above parameters allow sufficient detail recognition in the data to detect subtle anomalies that may represent mineralization and/or rocks of different lithological and petrophysical composition.

A base magnetometer to monitor diurnal variations in the magnetic field was located at the helicopter bases. The GEM GSM-19 base station magnetometer data were recorded once every 3 seconds. The CPU clock of the base magnetometer and the helicopter magnetometer were both synchronized to UTC (Universal Time Coordinates) through the built-in GPS receiver to allow correction of diurnals.

The navigation system uses GPS/GLONASS satellite tracking systems to provide real-time WGS-84 coordinate locations for every second. The accuracy achieved with no differential corrections is reported to be ± 5 m in the horizontal directions. The GNSS receiver antenna was mounted internally inside the canopy of the helicopter.

For quality control, the electromagnetic, magnetic, and radiometric, altitude and navigation data were monitored on four separate windows in the operator's display during flight, while they were recorded in three data ASCII streams to the PC hard disk drive. Spectrometry data were also recorded to an internal flash drive of the spectrometer. The data files were transferred to the field workstation via a USB flash drive. The raw data files were backed up onto the USB flash drive in the field.

2.2 Airborne survey instrumentation

Instrument specifications are given in Table 2. A Eurocopter AS350-B3 helicopter with the geophysical instruments installed and NGU's EM bird are shown in Figure 2. Frequencies and coil configurations for the Hummingbird EM system are given in Table 3.

Table 2. Instrument Specifications

Instrument	Producer / Model	Accuracy / Sensitivity	Sampling frequency / interval
Magnetometer	Scintrex Cs-2	<2.5nT throughout range / 0.0006nT √Hz rms	5 Hz
Base magnetometer	GEM GSM-19	0.1 nT	3 s
Electromagnetic	Geotech Hummingbird	1 – 2 ppm	10 Hz
Gamma spectrometer	Radiation Solutions RSX-5	1024 channels, 16 litres down, 4 litres up	1 Hz
Radar altimeter	Thales Communications AHV1600	± 5 ft 40 – 100 feet ± 5 % 100 – 500 feet ± 7 % 500 – 2500 feet	1 Hz
Pressure/temperature	Honeywell PPT	± 0.03 % FS	1 Hz
Navigation	Topcon GPS-receiver	± 5 meters	1 Hz
Acquisition system	NGU custom software		

Figure 2: Survey helicopter with a pilot and NGU Hummingbird EM system.

Table 3. Hummingbird EM system, frequency, and coil configurations

Coils	Frequency (Hz)	Orientation	Separation (m)
A	7001	Coaxial	6.30
B	6600	Coplanar	6.30

C	980	Coaxial	6.025
D	880	Coplanar	6.025
E	34133	Coplanar	4.90

2.3 Airborne Survey Logistics

The survey planning was done by Frode Ofstad. The field data quality control was performed by Frode Ofstad, Tom Kristiansen and Marie-Andrée Dumais. Data acquisition was done by field geophysicists from NGU. Pilots from Pegasus Helicopter in 2022 and 2023, and Airlift in 2024 were responsible for the helicopter operations. A summary of the survey specifications is shown in Table 4.

Table 4. Survey specifications:

Parameter	Specifications
Traverse (survey) line spacing	200 m
Traverse line direction	NW-SE (145º)
Nominal aircraft ground speed	65 – 143 km/h
Average aircraft ground speed	69 km/h
Average sensor terrain clearance – magnetic and EM	56 m
Average sensor terrain clearance - radiometric	86 m

3. DATA PROCESSING AND PRESENTATION

All processing and final products were performed at NGU. The ASCII data files were loaded into three separate Oasis Montaj databases. The datasets were processed consequently according to processing flow charts shown in Appendix A1, A2 and A3. The magnetic, electromagnetic and the spectrometry data were processed by Frode Ofstad. The maps were produced by Frode Ofstad, and the report was written by Frode Ofstad, based on the new Universal Publishing Formatting standard at NGU.

3.1 Total Field Magnetic Data

At the first stage the raw magnetic data were visually inspected, and spikes were removed manually. Non-linear filter was also applied to airborne raw data to eliminate short-period spikes. Typically, several corrections must be applied to magnetic data before gridding - heading correction, lag correction and diurnal correction.

3.1.1 Diurnal corrections

The temporal fluctuations in the magnetic field of the earth affect the total magnetic field readings recorded during the airborne survey. These are commonly referred to as magnetic diurnal variations. These fluctuations can be effectively removed from the airborne magnetic dataset by using a stationary reference magnetometer called base station that records the magnetic field of the earth simultaneously in a near location from the survey.

Diurnal magnetic variations were measured with GEM GSM-19 magnetometer. The base station computer clock was continuously synchronized with GPS clock. The base station magnetometer data were inspected for spikes and cultural noise. Both were removed manually if necessary. The data are reduced for the average base magnetic value for the survey to obtain the so-called magnetic diurnal.

The airborne magnetic data are corrected for the diurnal variation by applying the correction according to equation 1.

$$\boldsymbol{B}_{Tc} = \boldsymbol{B}_T + (\bar{B}_B - \boldsymbol{B}_B) \quad (1)$$

Where the variables are defined as followed:

$\mathbf{B}_{Tc}$: corrected airborne total field readings,

$\mathbf{B}_{T}$: airborne total field readings,

$\bar{B}_B$: average magnetic base level,

$\mathbf{B}_B$: magnetic base station readings.

The average datum base nT level ($\overline{B}_{\mathrm{B}}$) was set to 52500 for the 2022 survey at Eide, 52200 in 2023 at Tusten, 52300 at Tusten in the spring of 2024, and 51450 in autumn of 2024 with the base at Vestnes. Through the survey, the magnetic diurnals were within the standard NGU specifications during the entire survey (Rønning 2013).

3.1.2 Lag and heading corrections.

Neither a lag nor a cloverleaf test was performed before the survey. According to previous reports the lag between logged magnetic data and the corresponding navigational data was 1-2 fiducials. These values were observed to have a negligible effect on the processed results. A heading error for a towed system is usually either very small or non-existent. No lag and heading corrections were applied.

3.1.3 Magnetic data processing, gridding, and presentation

The total field magnetic anomaly data ($\boldsymbol{B}_{TA}$) were calculated from the diurnal corrected data ($\boldsymbol{B}_{Tc}$) after subtracting the IGRF for the surveyed area calculated for the data period (eq. 2)

$$\boldsymbol{B}_{TA} = \boldsymbol{B}_{Tc} - IGRF \qquad (2)$$

IGRF 2020 model was employed in these calculations, to ensure that the data set would match the previously processed and earlier published surrounding data sets.

The total field anomaly data were split into lines and then gridded using a minimum curvature method with a grid cell size of 50 meters. This cell size is exactly one quarter of the 200 meters average line spacing. To remove small line-to-line levelling errors that were detected on the gridded magnetic anomaly data, a micro-levelling technique was applied on the flight line based magnetic database. Finally, the micro-levelled data were gridded using minimum curvature method with 50 meters grid cell size.

The processing steps of magnetic data presented above were performed on a point basis. The following steps are performed on a grid basis.

The horizontal and vertical gradient along with the tilt derivative of the total magnetic anomaly were calculated from the micro-levelled total magnetic anomaly grid. The magnitude of the horizontal gradient was calculated according to equation 3:

$$HG = \sqrt{\left(\frac{\partial(B_{TA})}{\partial x}\right)^2 + \left(\frac{\partial(B_{TA})}{\partial y}\right)^2} \qquad (3)$$

where $\boldsymbol{B}_{TA}$ is the micro-levelled total field anomaly field. The vertical gradient (VG) was calculated by applying a vertical derivative convolution filter to the micro-levelled $\boldsymbol{B}_{TA}$field. The tilt derivative (TD) was calculated according to the equation 4:

$$TD = tan^{-1}\left(\frac{VG}{HG}\right) \qquad (3)$$

A 3x3 convolution filter was applied to smooth the resulting magnetic grids. The results are collected in a common database, gridded and presented as 40% transparent coloured shaded relief grids on top of topographic maps (1:200,000) using a histogram equalization stretch to help visualizing the full range of frequencies contained in the data. The maps are:

- Total field magnetic anomaly,
- Horizontal gradient of total magnetic anomaly,
- Vertical gradient of total magnetic anomaly,
- Tilt derivative (or Tilt angle) of the total magnetic anomaly.

The maps are representative of the distribution of magnetization over the surveyed areas. The list of the produced maps is shown in Table 6.

Noise in the 2023 magnetic data were filtered out in the processing. Some linear effects are still visible, mostly in the derivative grids, but it should not affect the geological interpretation of the magnetic data. Also, the merging of the five different datasets can produce some linear effects in the adjoining borders of the different survey areas.

3.2 Electromagnetic data

The EM system transmits five fixed frequencies and records an in-phase (IP) and a quadrature (Q) response for each of the five coil sets of the electromagnetic system. The received signals are processed and used for calculation of apparent resistivity.

To remove the effects of instrument drift caused by gradual temperature variations in the transmitting and receiving circuits, background responses are recorded during each flight. To obtain a background level, the bird is raised to an altitude of at least 800 ft above the topographic surface so that no electromagnetic responses from the ground are present in the recorded traces.

The EM traces observed at this altitude correspond to a background (zero) level of the system. If these background levels are recorded at 20-30 minutes interval, then the linear drift of the system can be removed on a flight-by-flight basis, before any further processing is carried out. Geosoft HEM module was used for applying drift correction. Residual instrumental drift, usually small, but non-linear, was manually removed manually on a line-to-line basis.

IP and Q data were filtered with non-linear filter to eliminate spherical spikes, which were represented as irregular noise of large amplitude in records and high frequency noise of bird electronics. Then, a low-pass filter was applied to suppress instrumental and cultural noise. These filters described in Appendix A2 were not able to suppress all the noise. Also, shifts in IP and Q data, with amplitude of 5-10 ppm, were observed in some flights. These shifts were edited manually where possible.

A 5-ppm amplitude-limited, 20 seconds non-linear filter was applied to the in-phase and quadrature signals. The non-linear filter result was then subtracted from each component before the inversion calculations. This ensures uniform data and clearer anomalies with fewer linear artifacts in the grids.

When final levelling of the EM data was complete, apparent resistivity was calculated from in-phase and quadrature EM components using a homogeneous half space model of the earth (Geosoft HEM module) for 7001, 6600, 980, 880 and 34133 Hz, using a threshold value of 2 ppm, starting inversion value of 1000 ohm-m, and fractional error of 1%.

Electromagnetic field decays rapidly with the distance (height of the sensors) as $[z^{-2} – z^{-5}]$ depending on the shape of the conductors and, at certain height, signals from the ground sources become comparable with instrumental noise. Levelling errors or precision of levelling can sometimes lead to appearance of artificial resistivity anomalies when data were collected at high instrumental altitude.

Application of threshold allows excluding such data from an apparent resistivity calculation, though not completely. It is particularly noticeable in low frequencies datasets. Apparent resistivity data were visually inspected; artificial anomalies associated with high altitude measurements were automatically removed. Data recorded at a height larger than 150 meters were considered as non-reliable and removed from presentation. Resistivity was gridded with a cell size of 50 meters. Power lines strongly affected low frequency data – 880 and 980 Hz frequencies, and the most prominent noise from large power lines were filtered.

The apparent resistivity grids from each year are presented as 30% transparent coloured grids on top of topographic maps (1:200,000) using a log-linear stretch to emphasize on the anomalies caused by conductor bodies. The list of the produced maps is shown in Table 6.

Due to equipment malfunctions, small parts of the 880Hz data are missing in the spring of 2024 survey, and some parts of 6,600Hz data are missing for the autumn of 2024 survey.

3.3 Radiometric data

Airborne gamma-ray spectrometry measures the abundance of potassium (K), thorium (Th), and uranium (U) in rocks and weathered materials by detecting gamma-rays emitted due to the natural radioelement decay of these elements. The data analysis method is based on the IAEA recommended method for U, Th and K (International Atomic Energy Agency, 1991; 2003). A short description of the individual processing steps of that methodology as adopted by NGU is given below.

3.3.1 Energy windows

The gamma-ray spectra were initially divided into standard energy windows corresponding to the individual radio-nuclides K, U and Th. Figure 3 shows an example of a Gamma-ray spectrum and the corresponding energy windows and radioisotopes (with peak energy in MeV) responsible for the radiation.

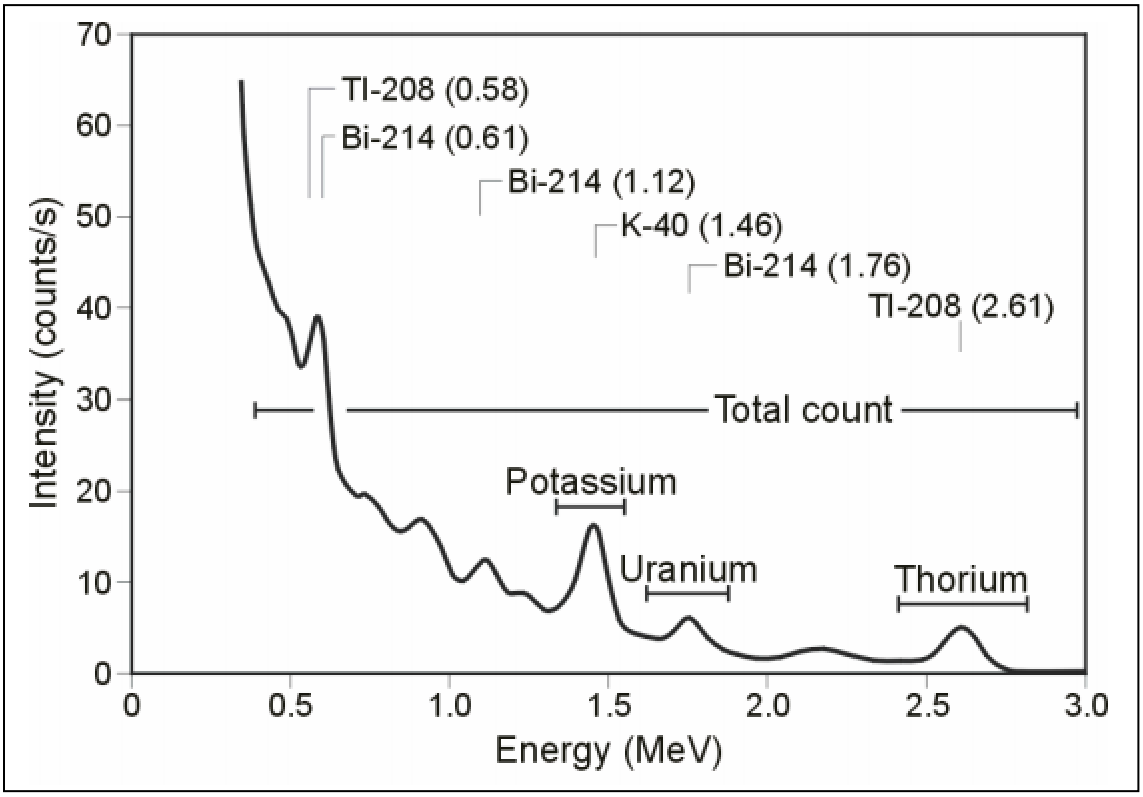

Figure 3: Gamma-ray spectrum with K, Th, U and Total Count windows.

The RSX-5 spectrometer is a 1024 channel system with four downward detectors and one upward looking detector, which means that the actual Gamma-ray spectrum is divided into 1024 channels. The first channel is reserved for "Live Time" and the last for cosmic radiation. Table 5 shows the windows that were used for data processing.

Table 5. Specified channel windows for the 1024 RSX-5 system.

Gamma-ray spectrum	Cosmic	Total count	K	U	Th
Downward	1023	137-937	457-523	553-620	803-937
Upward	1023			553-620	
Energy (MeV)	>3.07	0.4-2.8	1.36-1.56	1.65-1.85	2.4-2.8

3.3.2 Live Time correction

The data were corrected for live time. "Live time" is an expression of the relative length of time the instrument was able to register new pulses per sample interval. On the other hand, "dead time" is an expression of the relative length of time the system was unable to register new pulses per sample interval. The relation between “dead time” and “live time” is given by the equation 5:

$$\text{“Live time”} = \text{“Real time”} - \text{“Dead time”} \tag{5}$$

where the “real time” or “acquisition time” is the elapsed time over which the spectrum is accumulated (about 1 000 000 µs).

The live time correction is applied to the total count, Potassium, Uranium, Thorium, upward Uranium, and cosmic windows. The formula used to apply the correction is as follows:

$$C_{LT} = C_{RAW} \cdot \frac{Acquisition\ Time}{Live\ Time} \tag{6}$$

where C_{LT} is the live time corrected window in counts per second, C_{RAW} is the raw window data in counts per second, while Acquisition Time and Live Time are in microseconds.

3.3.3 Cosmic and aircraft correction

Background radiation resulting from cosmic rays and aircraft contamination was removed from the total count, potassium, uranium, thorium, upward uranium windows using the following formula:

$$C_{CA} = C_{LT} - (a_c + b_c \cdot C_{Cos}) \tag{7}$$

where C_{CA} is the cosmic and aircraft corrected window, C_{LT} is the live time corrected window, a_c is the aircraft background for this window, b_c is the cosmic stripping coefficient for this window and C_{Cos} is the low pass filtered cosmic window. Cosmic and aircraft background coefficients were determined during the high-altitude calibration flight performed on September 6th and 9th 2023 in Verdal.

3.3.4 Radon correction

The upward detector method, as discussed in IAEA (1991), was applied to remove the effects of the atmospheric radon in the air below and around the helicopter. Using spectrometry data over-water, where there is no contribution from the ground sources, enables the calculation of the coefficients (a_c and b_c) for the linear equations that relate the cosmic corrected counts per second of the Uranium window with the total count, potassium, thorium, and uranium upward windows over water. Data over-land was used in conjunction with data over-water to calculate the a_1 and a_2 coefficients used in equation 8 for the determination of the radon component in the downward uranium window:

$$U_r = \frac{Uup_{CA} - a_1 \cdot U_{CA} - a_2 \cdot Th_{CA} + a_2 \cdot b_{Th} - b_U}{a_U - a_1 - a_2 \cdot a_{Th}} \tag{8}$$

where U_r is the radon component in the downward uranium window, Uup_{CA} is the filtered upward uranium, U_{CA} is the filtered uranium, Th_{CA} is the filtered thorium, a_1, a_2, a_U and a_{Th} are proportional factors and b_{Th} and b_U are constants determined experimentally.

The effects of radon in the downward uranium are removed by simply subtracting U_r from U_{CA}. The effects of radon in the other windows are removed using the following formula:

$$C_{RC} = C_{CA} - (a_C \cdot U_r + b_C) \tag{9}$$

where C_{RC} is the radon corrected window, C_{CA} is the cosmic and aircraft corrected window, U_r is the radon component in the downward uranium window, a_C is the proportionality factor and b_C is the constant determined experimentally for this window from over-water data.

3.3.5 Compton stripping

Radon corrected potassium, uranium and thorium windows are subjected to spectral overlap correction. Compton scattered gamma rays in the radio-nuclides energy windows were corrected by window stripping using Compton stripping ratios determined from measurements on calibrations pads (Grasty et al, 1991) at the Geological Survey of Norway in Trondheim performed on October 25th, 2023 (see values in Appendix A2).

The stripping corrections are given by the following formulas:

$$A_1 = 1 - (g \cdot \gamma) - (a \cdot \alpha) + (a \cdot g \cdot \beta) - (b \cdot \beta) + (b \cdot \alpha \cdot \gamma) \tag{10}$$

$$U_{ST} = \frac{Th_{RC} \cdot \big((g \cdot \beta) - \alpha\big) + U_{RC} \cdot (1 - b \cdot \beta) + K_{RC} \cdot \big((b \cdot \alpha) - g\big)}{A_1} \tag{11}$$

$$Th_{ST} = \frac{Th_{RC} \cdot \big(1 - (g \cdot \gamma)\big) + U_{RC} \cdot (b \cdot \gamma - a) + K_{RC} \cdot \big((a \cdot g) - b\big)}{A_1} \tag{12}$$

$$K_{ST} = \frac{Th_{RC} \cdot \big((\alpha \cdot \gamma) - \beta\big) + U_{RC} \cdot \big((a \cdot \beta) - \gamma\big) + K_{RC} \cdot \big(1 - (a \cdot \alpha)\big)}{A_1} \tag{13}$$

where Th_{RC}, U_{RC} and K_{RC} are the radon corrected uranium, thorium, and potassium and a, b, g, α, β and γ are the Compton stripping ratios, determined from measurements on calibration pads. U_{ST}, Th_{ST} and K_{ST} are stripped values of uranium, thorium, and potassium.

3.3.6 Reduction to standard temperature and pressure

The radar altimeter data were converted to effective height (H_{STP}) using the acquired temperature and pressure data, according to the expression:

$$H_{STP} = H \cdot \frac{273.15}{T + 273.15} \cdot \frac{P}{1013.25} \tag{14}$$

where H is the B-spline (basis spline) smoothed observed radar altitude in meters, T is the measured air temperature in degrees Celsius and P is the measured barometric pressure in millibars.

3.3.7 Height attenuation correction

Variations caused by changes in the aircraft altitude relative to the ground were corrected to a nominal height of 60 meters. Data recorded at a height larger than 150 meters were considered as non-reliable and removed from processing. Total count, uranium, thorium, and potassium stripped windows were subjected to height attenuation correction according to the equation:

$$C_{60m} = C_{ST} \cdot e^{C_{ht} \cdot (60 - H_{STP})} \tag{15}$$

where C_{ST} is the stripped corrected window, C_{ht} is the height attenuation coefficient for that window, determined from calibration flights, and H_{STP} is the effective height.

3.3.8 Conversion to ground concentrations

Finally, corrected count rates were converted to effective ground element concentrations using calibration values derived from calibration pads (Grasty et al, 1991) at the Geological Survey of Norway in Trondheim performed on October 25th, 2023 (see values in Appendix A3). The corrected data provide an estimate of the apparent surface concentrations of potassium, equivalent uranium, and equivalent thorium (K, eU and eTh). Potassium concentration is expressed as a percentage, equivalent uranium, and thorium as parts per million (ppm). Uranium and thorium are described as “equivalent” since their presence is inferred from gamma-ray radiation from daughter elements (^{214}Bi for uranium, ^{208}Tl for thorium). The concentration of the elements (C_{CONC}) is calculated according to the following expressions:

$$C_{CONC} = C_{60m} / C_{SENS\_60m} \tag{16}$$

Where C_{60m} is the height corrected window, C_{SENS_60m} is experimentally determined sensitivity reduced to the nominal height (60m).

3.3.9 Spectrometry data gridding and presentation

Gamma-rays from potassium, thorium and uranium emanate from the uppermost 30 to 40 centimetres of soil and rock in the crust (Minty, 1997). Variations in the concentrations of these radioactive elements are largely related to changes in the mineralogy and geochemistry of the Earth’s surface.

The spectrometry data were stored in a database and the ground concentrations were calculated following the processing steps. A list of the parameters used in these steps is given in Appendix A3.

Then the data were split in lines and ground concentrations of the three main natural radio-elements potassium, thorium and uranium and total gamma-ray flux (total count) were gridded using a minimum curvature method with a grid cell size of 50 meters.

Quality of the radiometric data was within standard NGU specifications (Rønning 2013). For further reading regarding standard processing of airborne radiometric data, we recommend the publications from Minty et al. (1997). A 3x3 convolution filter was applied to smooth the concentration grids. The radiometric grids from the different areas were gridded separately and stitched, then presented as 30% transparent coloured shaded relief grids on top of topographic maps (1:200000) using a linear stretch. The list of the produced maps is shown in Table 6.

4. PRODUCTS

Processed digital data from the survey are presented as:

- Geosoft databases are available upon request,
- Geosoft grids are available for download on the Geoscience portal (Er Mapper or Geosoft format),
- Maps are available in pdf format upon request.

Table 6. Maps in scale 1:100000, available from NGU upon request.

Map #	Name
2024.036-00	Survey Flight Path
2024.036-01	Total magnetic field
2024.036-02	Magnetic Horizontal Gradient
2024.036-03	Magnetic Vertical Gradient
2024.036-04	Magnetic Tilt Derivative
2024.036-05	Apparent resistivity, Frequency 7001 Hz, coaxial coils
2024.036-06	Apparent resistivity, Frequency 6600 Hz, coplanar coils
2024.036-07	Apparent resistivity, Frequency 980 Hz, coaxial coils
2024.036-08	Apparent resistivity, Frequency 880 Hz, coplanar coils
2024.036-09	Apparent resistivity, Frequency 34133 Hz, coplanar coils
2024.036-10	Radiometric Total counts
2024.036-11	Potassium ground concentration
2024.036-12	Uranium ground concentration
2024.036-13	Thorium ground concentration
2024.036-14	Radiometric Ternary Image

Downscaled images of the maps are shown in figures 4 to 18.

5. REFERENCES

IAEA 1991: Airborne Gamma-Ray Spectrometry Surveying, Technical Report No 323, Vienna, Austria, 97 pp.

Geotech 1997: Hummingbird Electromagnetic System. User manual. Geotech Ltd. October 1997

Grasty, R.L., Holman, P.B. & Blanchard 1991: Transportable Calibration pads for ground and airborne Gamma-ray Spectrometers. Geological Survey of Canada. Paper 90-23. 62 pp.

IAEA 2003: Guidelines for radioelement mapping using gamma ray spectrometry data. IAEA-TECDOC-1363, Vienna, Austria. 173 pp.

Minty, B.R.S., Luyendyk, A.P.J. and Brodie, R.C. 1997: Calibration and data processing for gamma-ray spectrometry. AGSO – Journal of Australian Geology & Geophysics. 17(2). 51-62.

Naudy, H. and Dreyer, H. 1968: Non-linear filtering applied to aeromagnetic profiles. Geophysical Prospecting. 16(2). 171-178.

Rønning, J.S. 2013: NGUs helikoptermålinger. Plan for sikring og kontroll av datakvalitet. NGU Intern rapport 2013.001. 38 pp.

APPENDIX A1: FLOW CHART OF MAGNETIC DATA PROCESSING

The meaning of parameters is described in the referenced literature.

Processing flow:

- Creation of database and quality control
- Visual inspection of airborne data and manual spike removal
- Import of diurnal data from base magnetometer database
- Correction of data for diurnal variation
- IGRF 2020 removed.
- Splitting flight data by lines
- Gridding
- Micro-levelling with 1200 m cutoff length, 50 m cell size, 800 m Naudy filter
- 3x3 convolution filter

APPENDIX A2: FLOW CHART OF ELECTROMAGNETIC DATA PROCESSING

The meaning of parameters is described in the referenced literature.

Processing flow:

- Automated levelling using Geosoft HEM module.
- Filtering of in-phase and quadrature channels with non-linear and low-pass filters

EM frequency (Hz)	A - 7001	B - 6606	C - 980	D - 880	E - 34133
Non-linear filter (fiducials)	10	10	15	15	15
Low-pass filter (fiducials)	20	20	20	30	30

- Quality control and visual inspection of data
- Manual removal of remaining part of instrumental drift
- Additional levelling using low-pass filter to reduce linear noise.
- Calculation of an apparent resistivity using in-phase and quadrature channels
- Splitting flight data by lines, Log-linear gridding with 3 to 12000 colour scale
- Resistivity data over water were removed.

APPENDIX A3: FLOW CHART OF RADIOMETRY DATA PROCESSING

Underlined processing stages are not only applied to the K, U and Th window, but also to the total count. The meaning of parameters is described in the referenced literature.

- Airborne and cosmic correction (IAEA, 2003): the parameters for data flown in 2022 were determined by high altitude calibration flights (1,500-9,000 ft) in Randsfjorden, October 2021. Verdal on September 6th and 9th, 2023.

Window	Background coefficients	Cosmic coefficients
K	6.5274	0.0537
U	4.3312	0.0373
Th	0	0.0694
U_{up}	1.1423	0.0108
Total counts	71.552	0.936

- the parameters for data flown in 2023-2024 were determined by high altitude calibration flights (1500-9000 ft) in Verdal on September 6th and 9th, 2023.

Window	Background coefficients	Cosmic coefficients
K	2.4143	0.0745
U	0	0.0622
Th	0	0.0696
U_{up}	0	0.017
Total counts	3.4613	1.2874

- Radon correction using upward detector method (IAEA, 2003): parameters determined from survey data over water and land in Møre og Romsdal 2022 for data from 2022.

Coefficient	Value	Coefficient	Value
a_u	0.69015	b_u	0.0477
a_K	1.14498	b_K	1.07347
a_{Th}	0.1023	b_{Th}	0.49752
a_{TC}	15.87281	b_{TC}	0
a_1	0.06160057	a_2	0.04123201

- Radon correction using upward detector method (IAEA, 2003): parameters determined from survey data over water and land in Møre og Romsdal 2023 for data from 2023 and 2024.

Coefficient	Value	Coefficient	Value
a_u	0.31971	b_u	0.73824
a_K	0.97694	b_K	2.27195
a_{Th}	0.04125	b_{Th}	0.43941
a_{TC}	18.24724	b_{TC}	7.3267
a_1	0.00785108	a_2	0.0866471

- Stripping corrections (IAEA, 2003): parameters determined from measurements on calibrations pads at NGU on October 25th, 2023, for the data from 2023 and 2024.

Stripping ratios	Values 2022	Values 2023/24
a	0.045493	0.046343
b	0	0
c	0	0
α	0.273125	0.269042
β	0.426343	0.427164
γ	0.771199	0.763561

- Height attenuation correction to a height of 60 m: parameters determined by several calibration flights at increased altitude (100 – 700 ft). The height attenuation coefficients (1/m) were calculated from the calibration performed in Verdal on September 6th, 2023, for the data flown in 2023-2024.

Window	Attenuation coefficients
K	-0.0086
U	-0.0071
Th	-0.0079
TC	-0.0077

- Converting counts at 60 m heights to element concentration on the ground: parameters determined from measurements on calibrations pads at NGU, 2021.

Window	Sensitivity coefficients
K (counts/%)	0.007344
U (counts/ppm)	0.086075
Th (counts/ppm)	0.151879

- Grids smoothening by a 3x3 convolution filtering (Oasis Montaj).

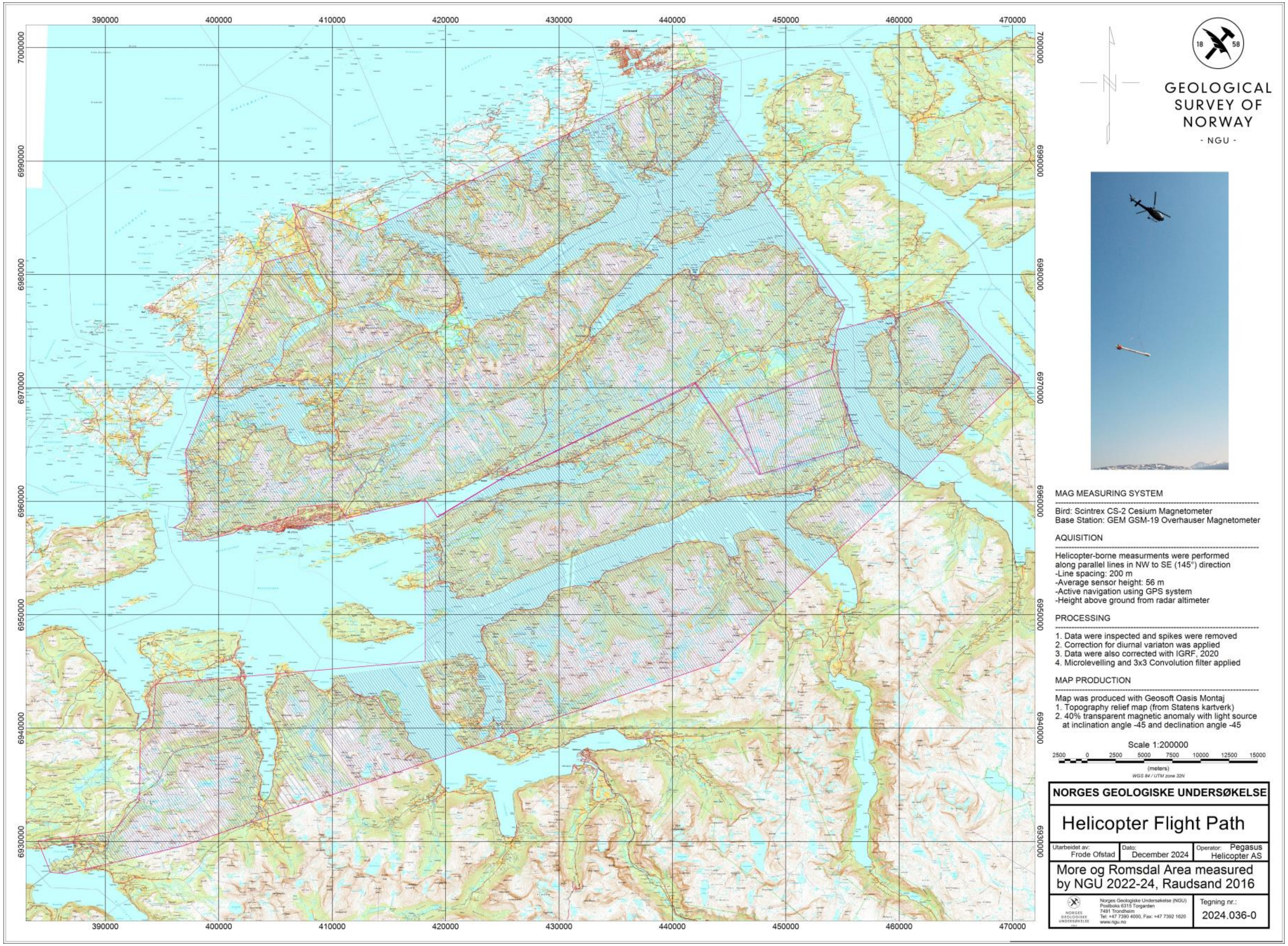

Figure 4: Møre og Romsdal selected survey area with flight path.

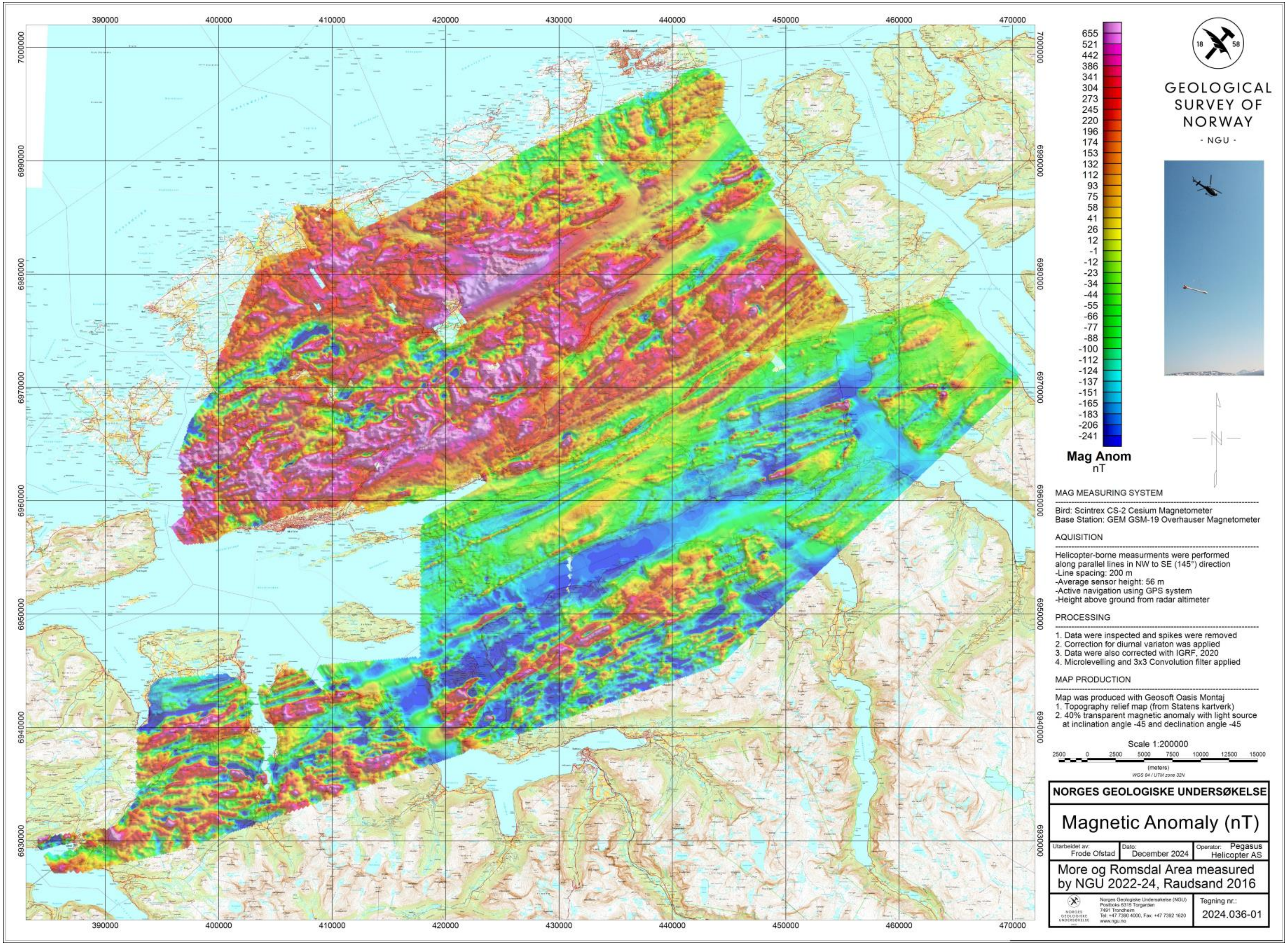

Figure 5: Total Magnetic Field.

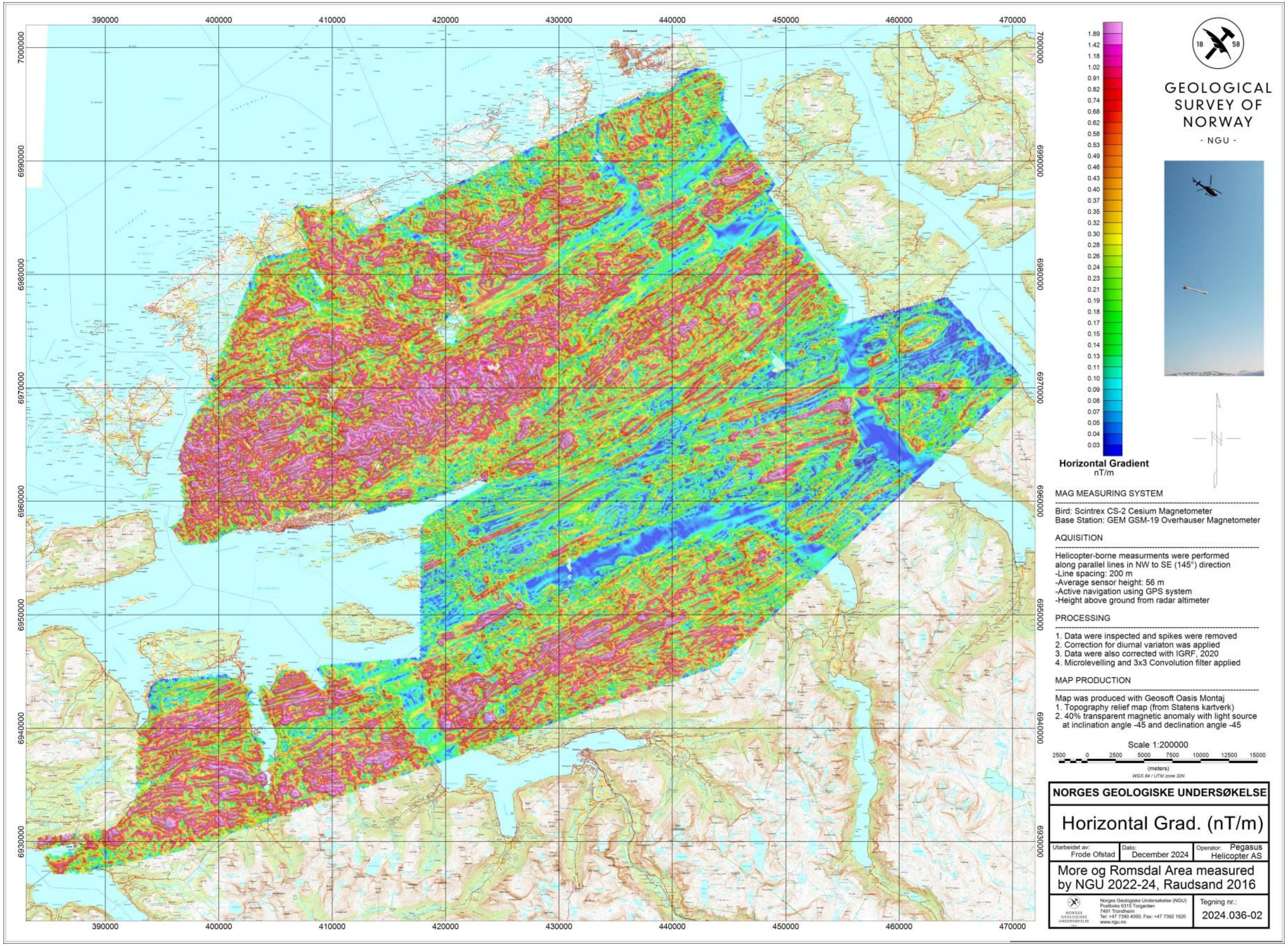

Figure 6: Magnetic Horizontal Gradient.

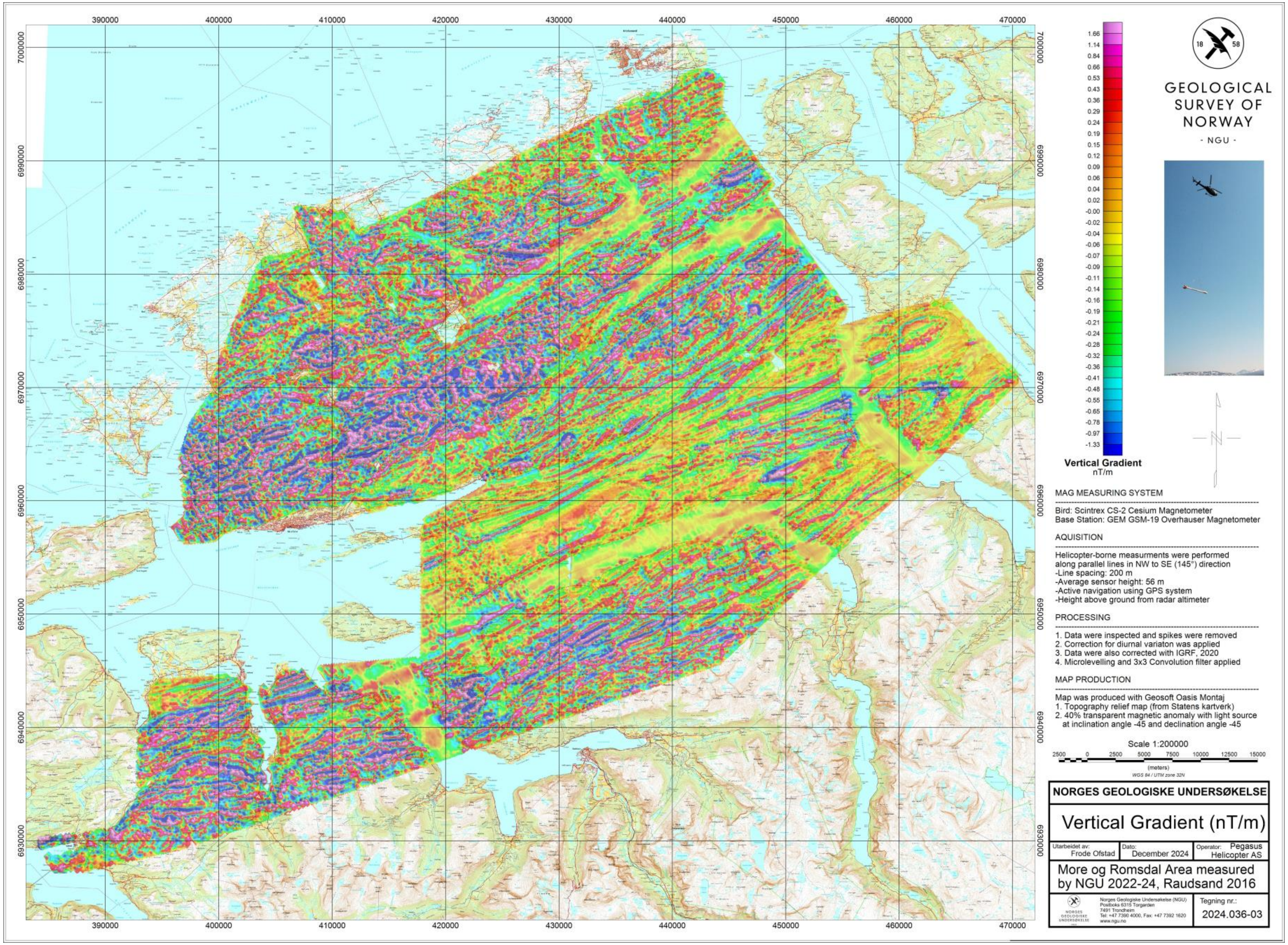

Figure 7: Magnetic Vertical Gradient.

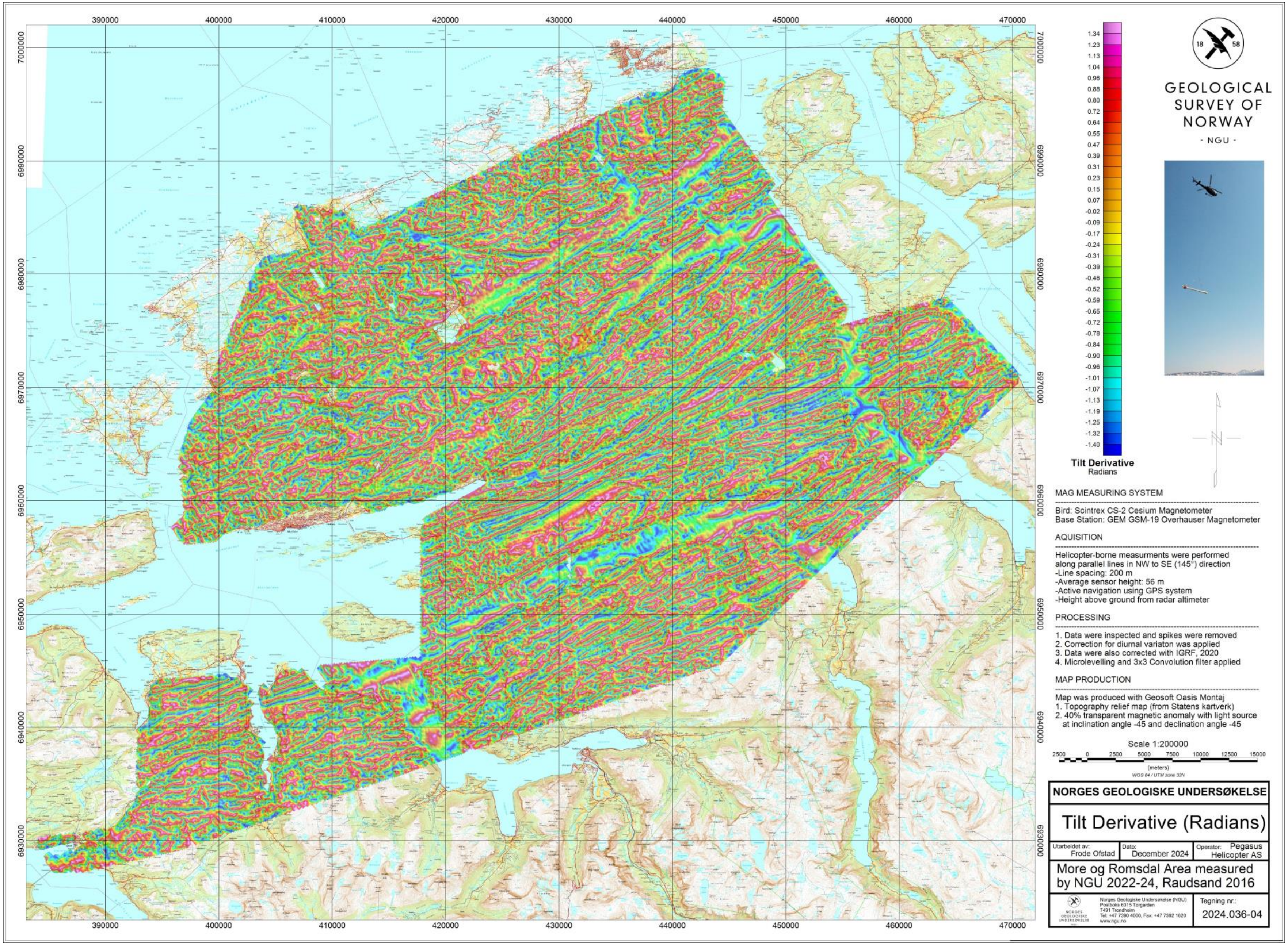

Figure 8: Magnetic Tilt Derivative.

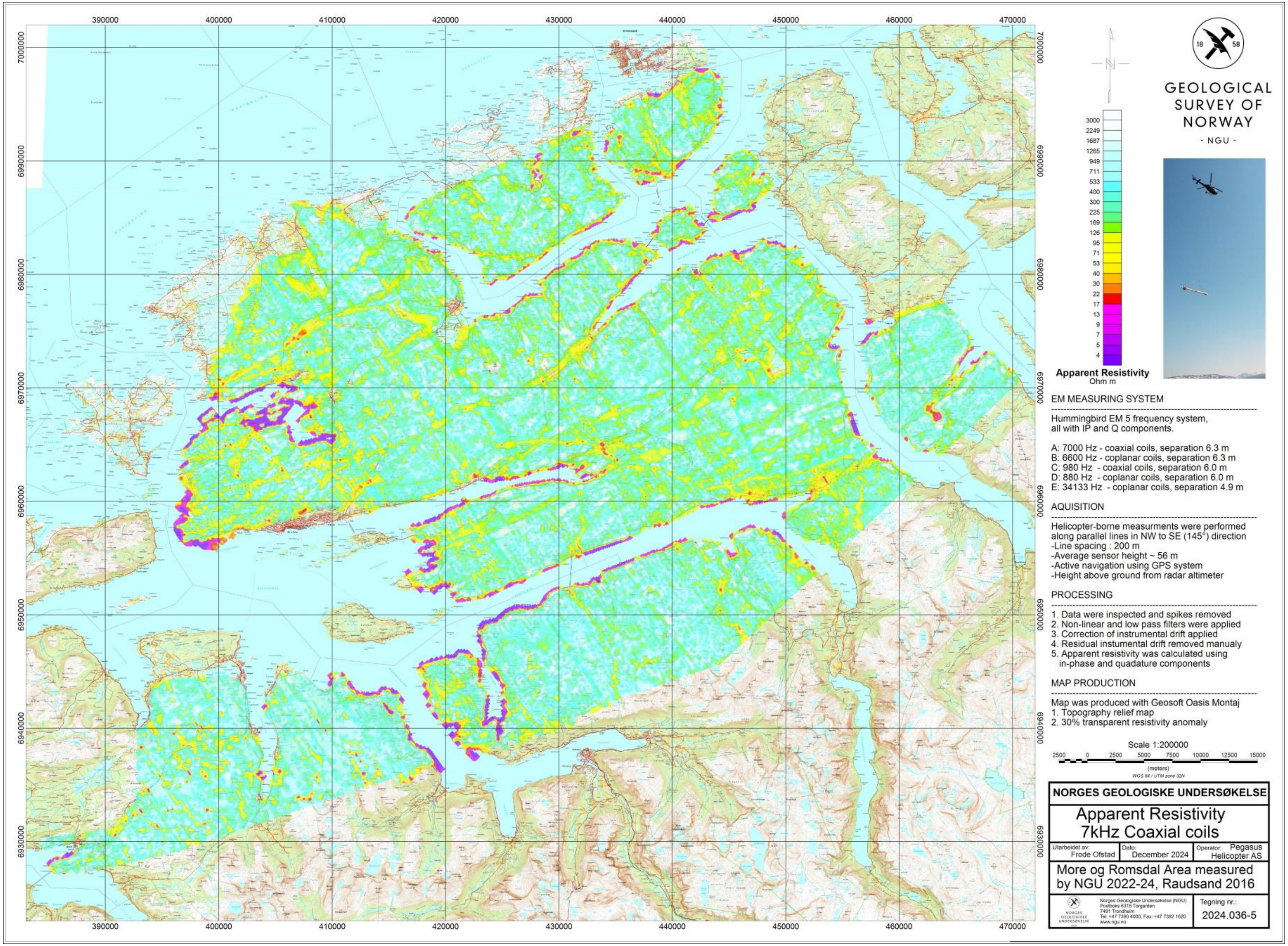

Figure 9: Apparent resistivity. Frequency 7000 Hz, Coaxial coils.

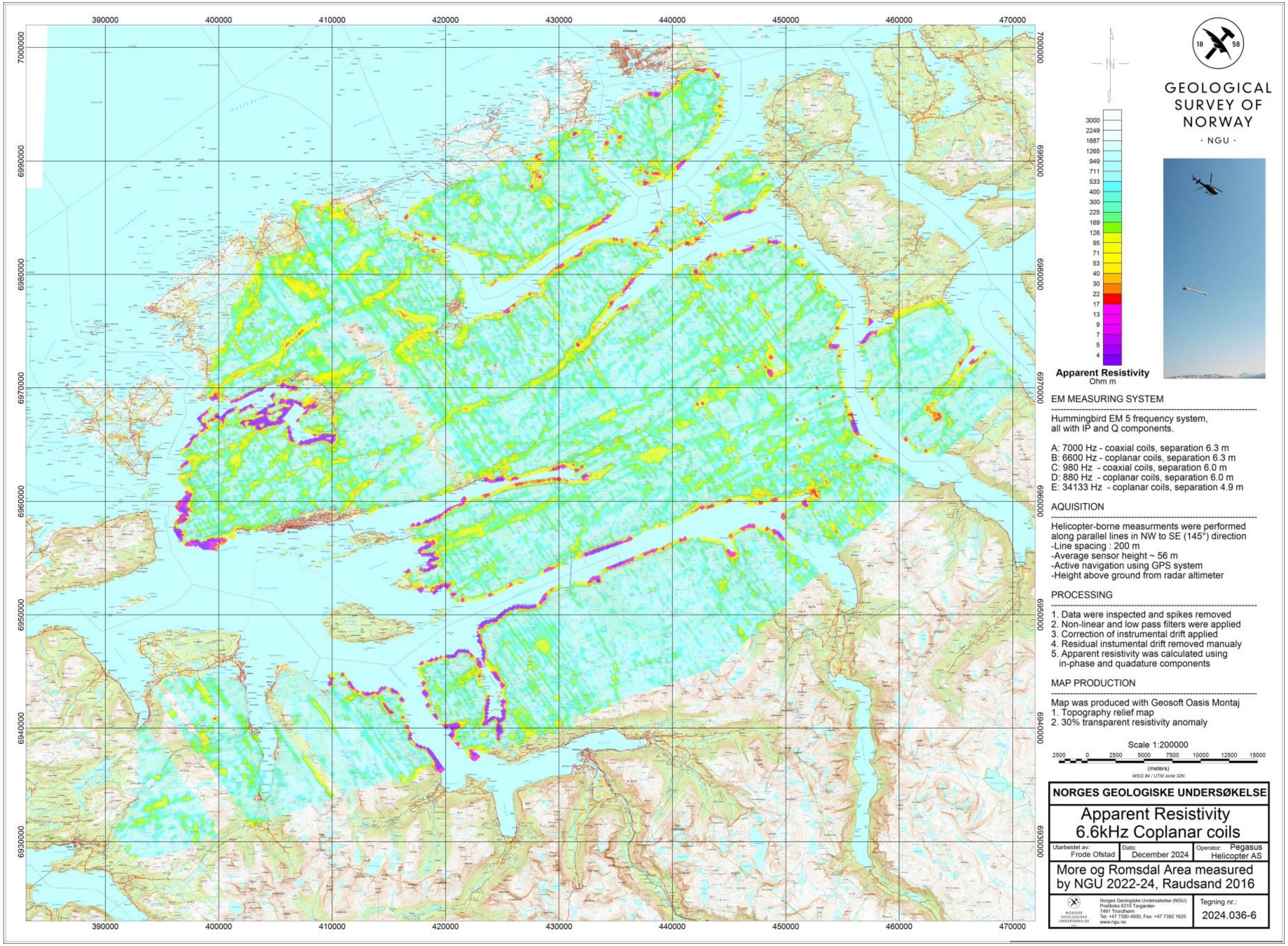

Figure 10: Apparent resistivity. Frequency 6600 Hz, Coplanar coils.

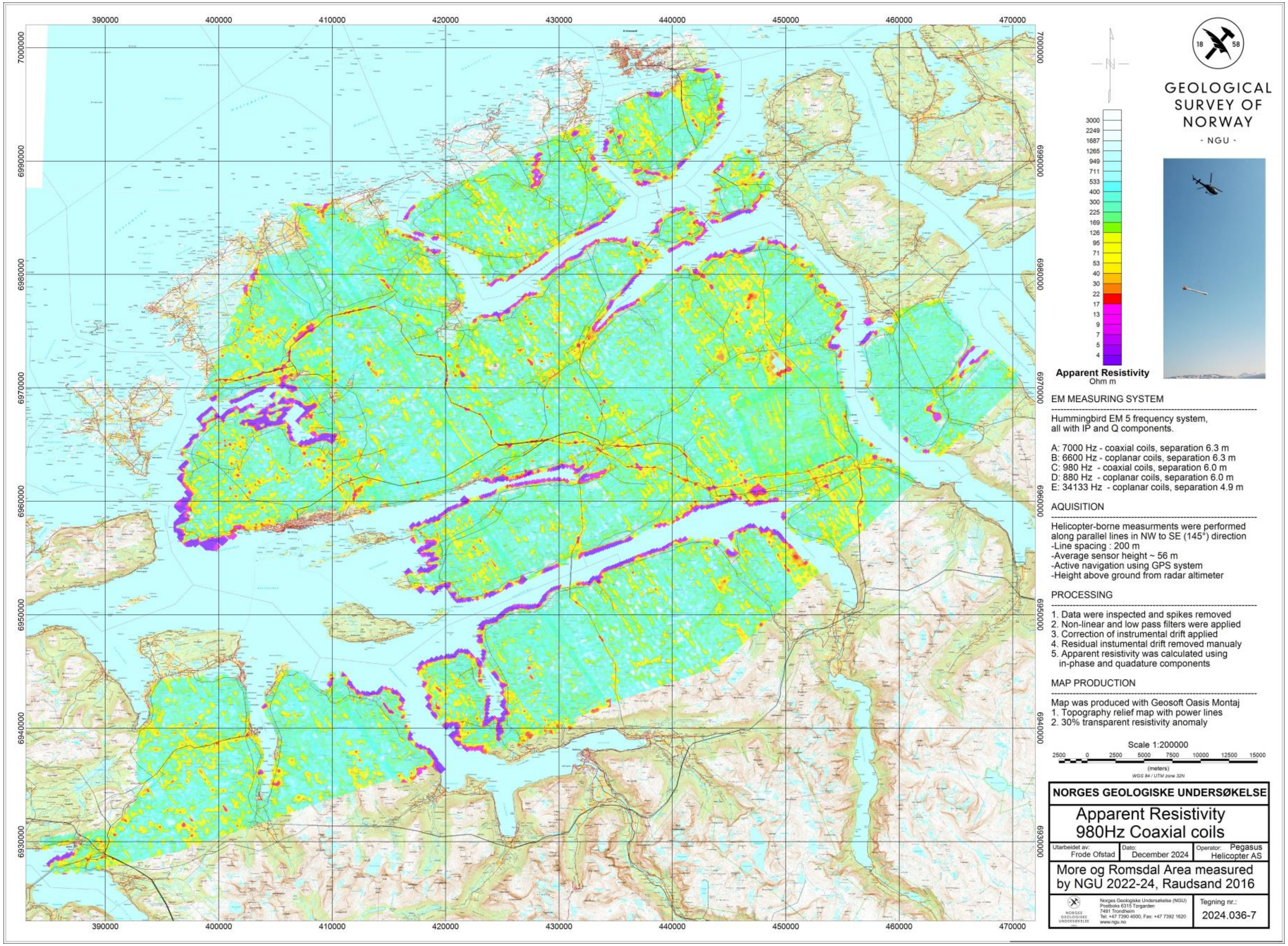

Figure 11: Apparent resistivity. Frequency 980 Hz, Coaxial coils.

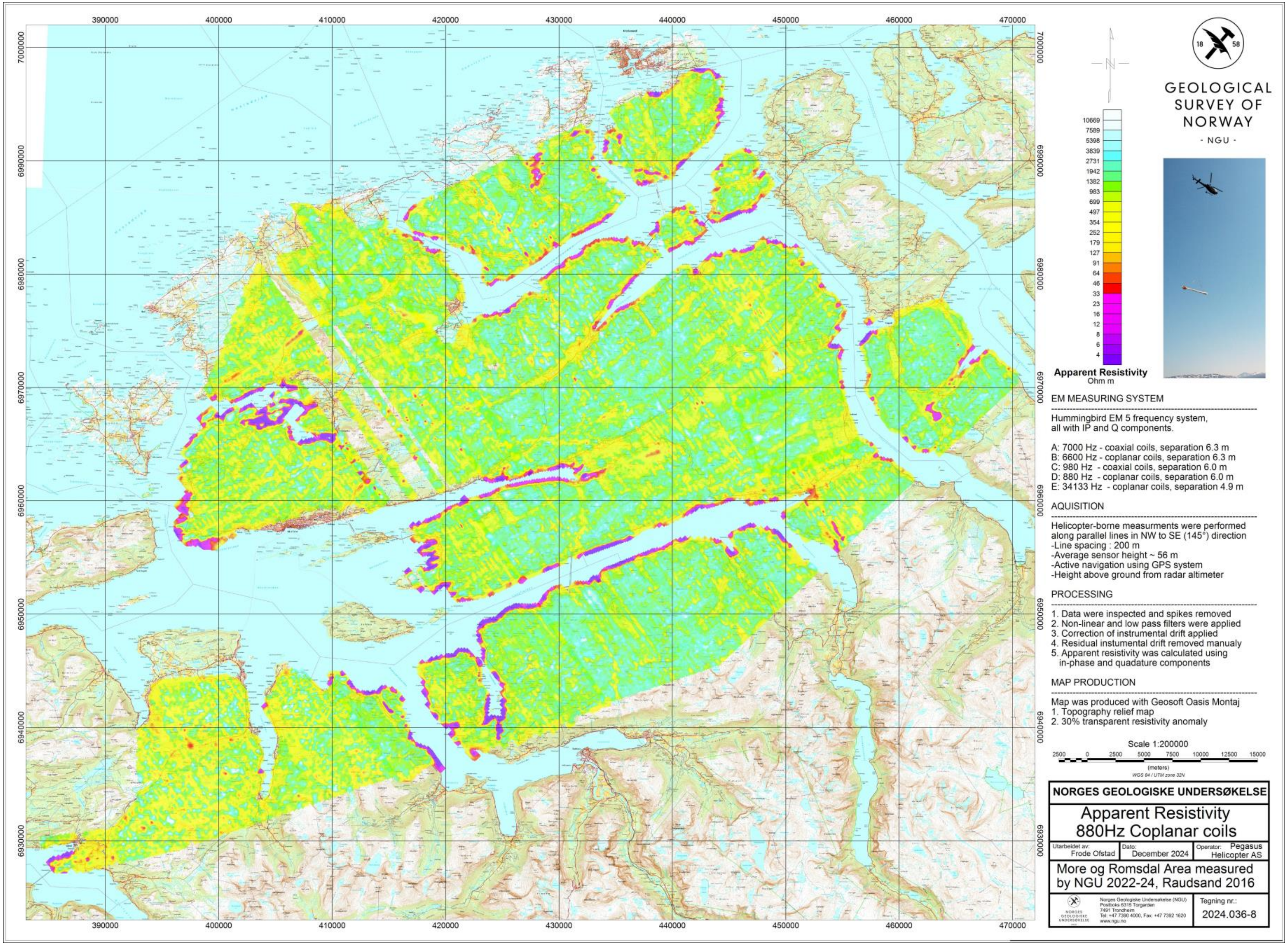

Figure 12: Apparent resistivity. Frequency 880 Hz, Coplanar coils.

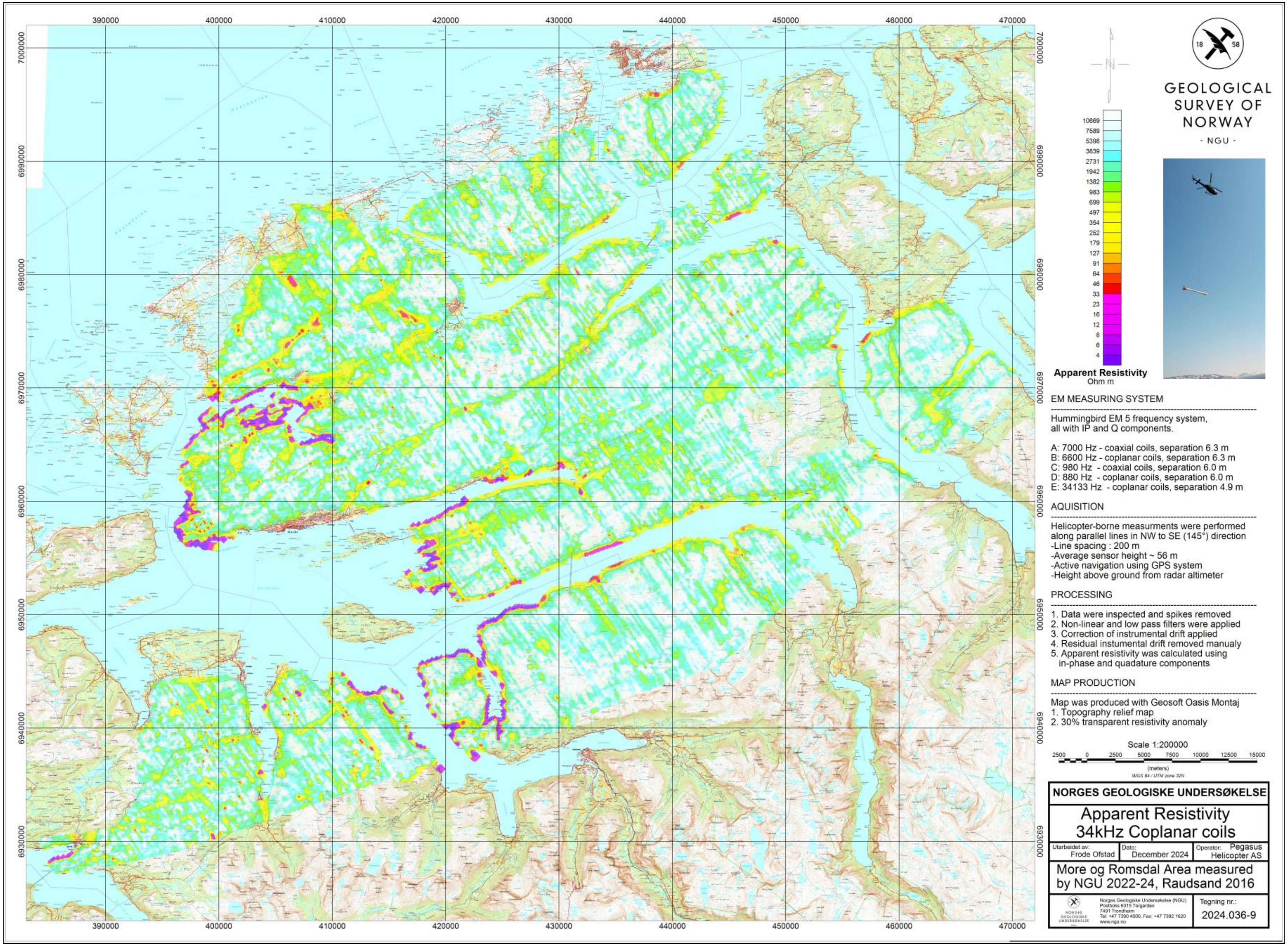

Figure 13: Apparent resistivity. Frequency 34133 Hz, Coplanar coils.

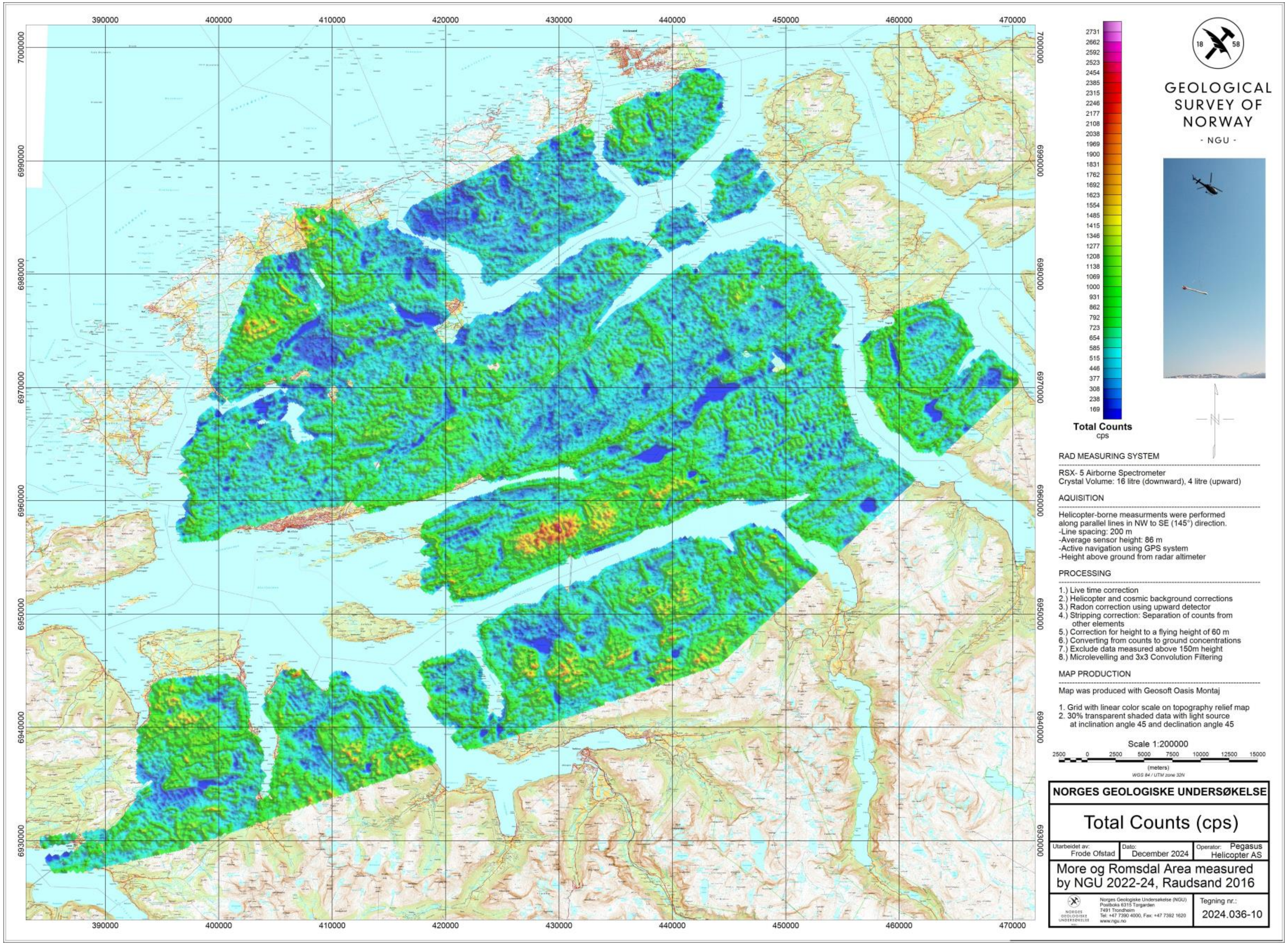

Figure 14: Radiometric Total Counts.

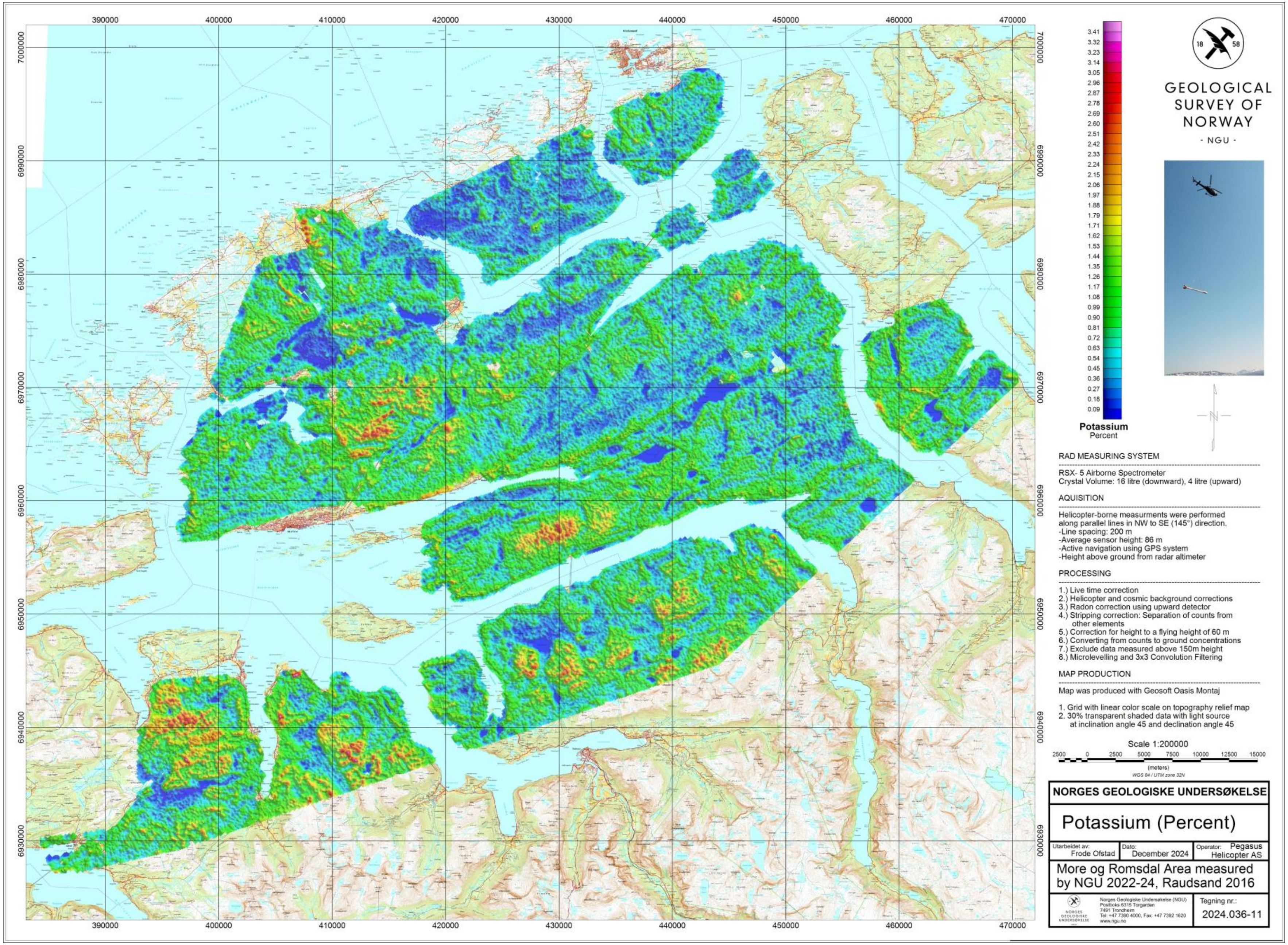

Figure 15: Potassium ground concentration.

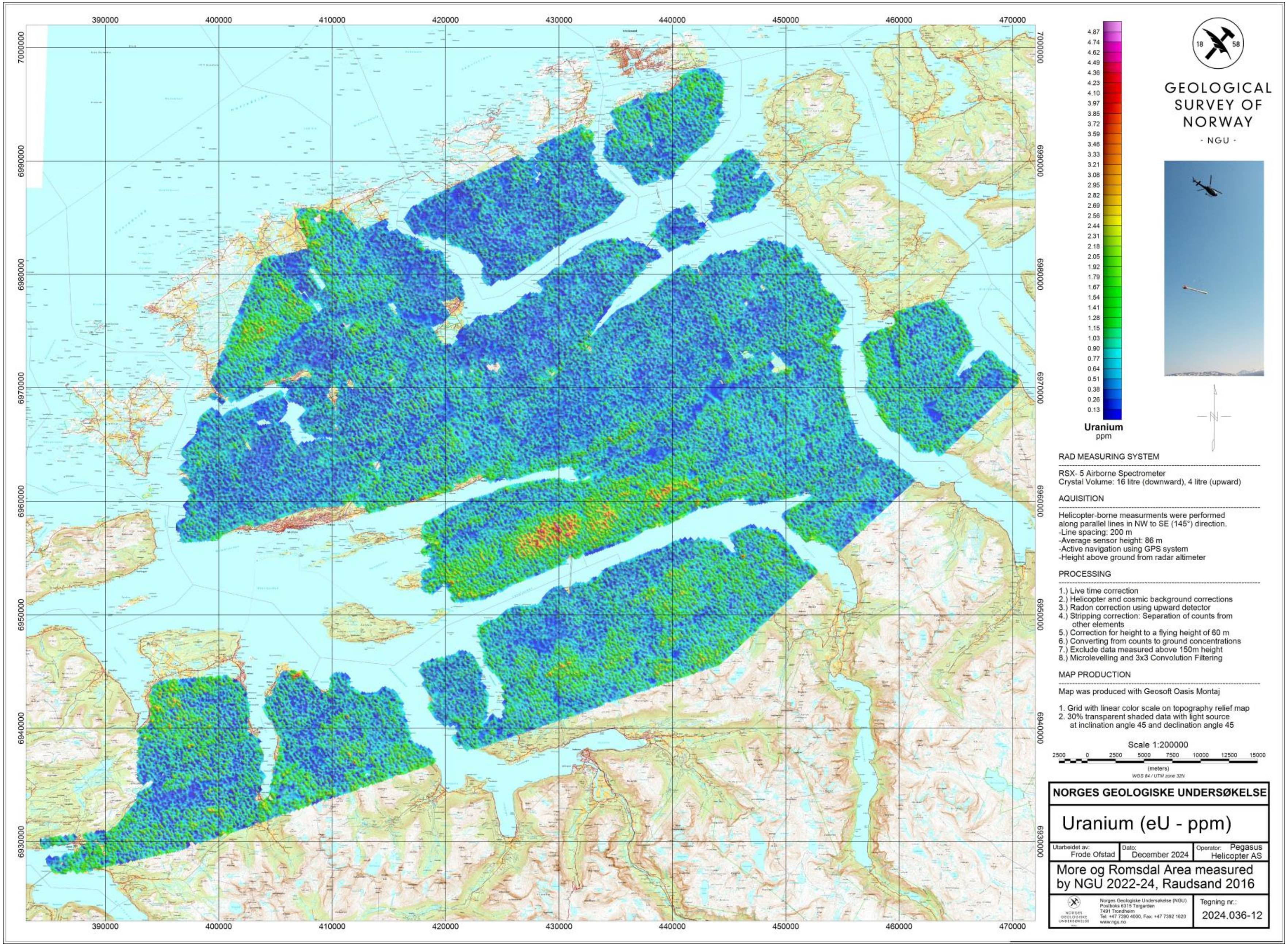

Figure 16: Uranium ground concentration.

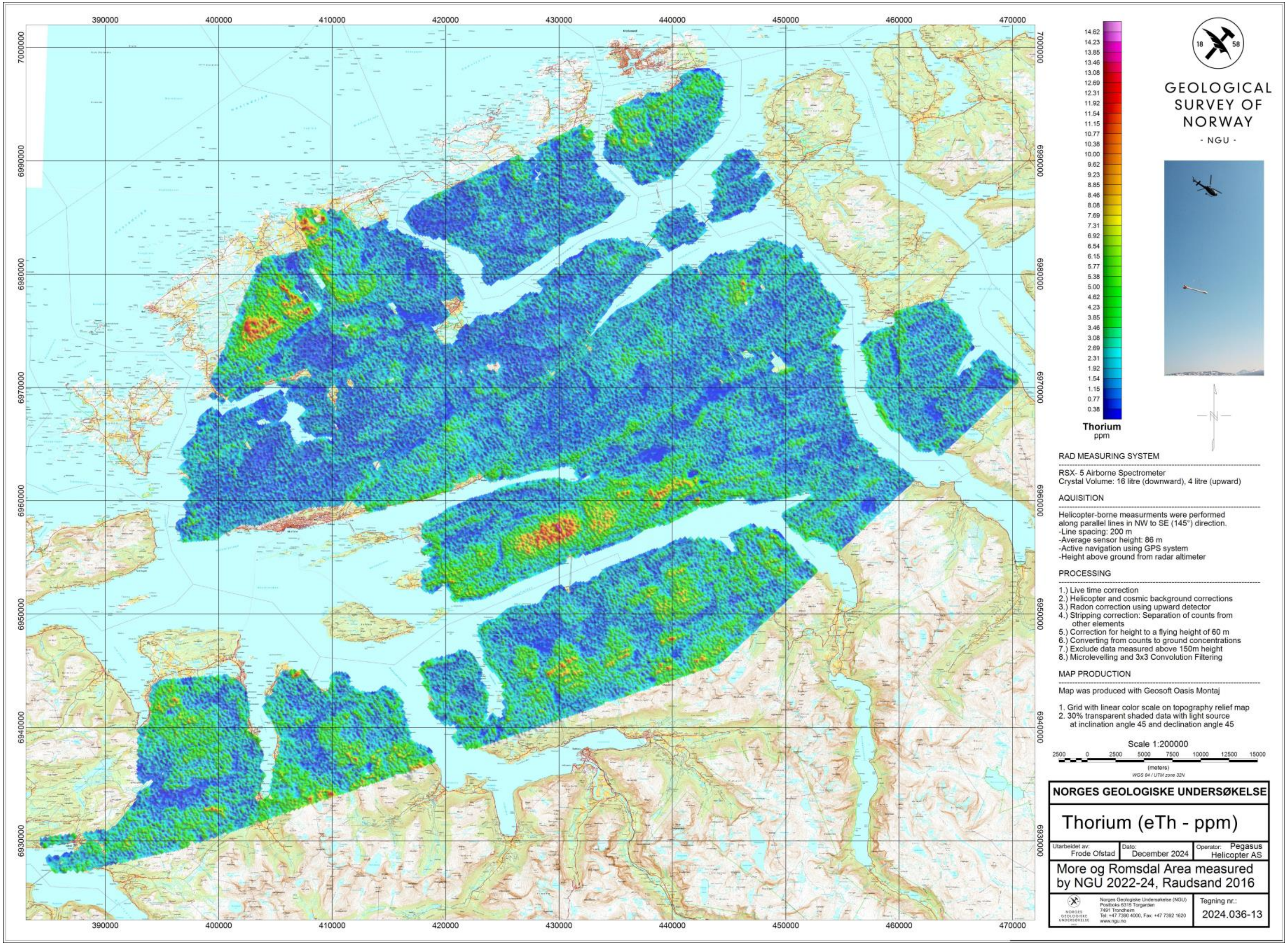

Figure 17: Thorium ground concentration.

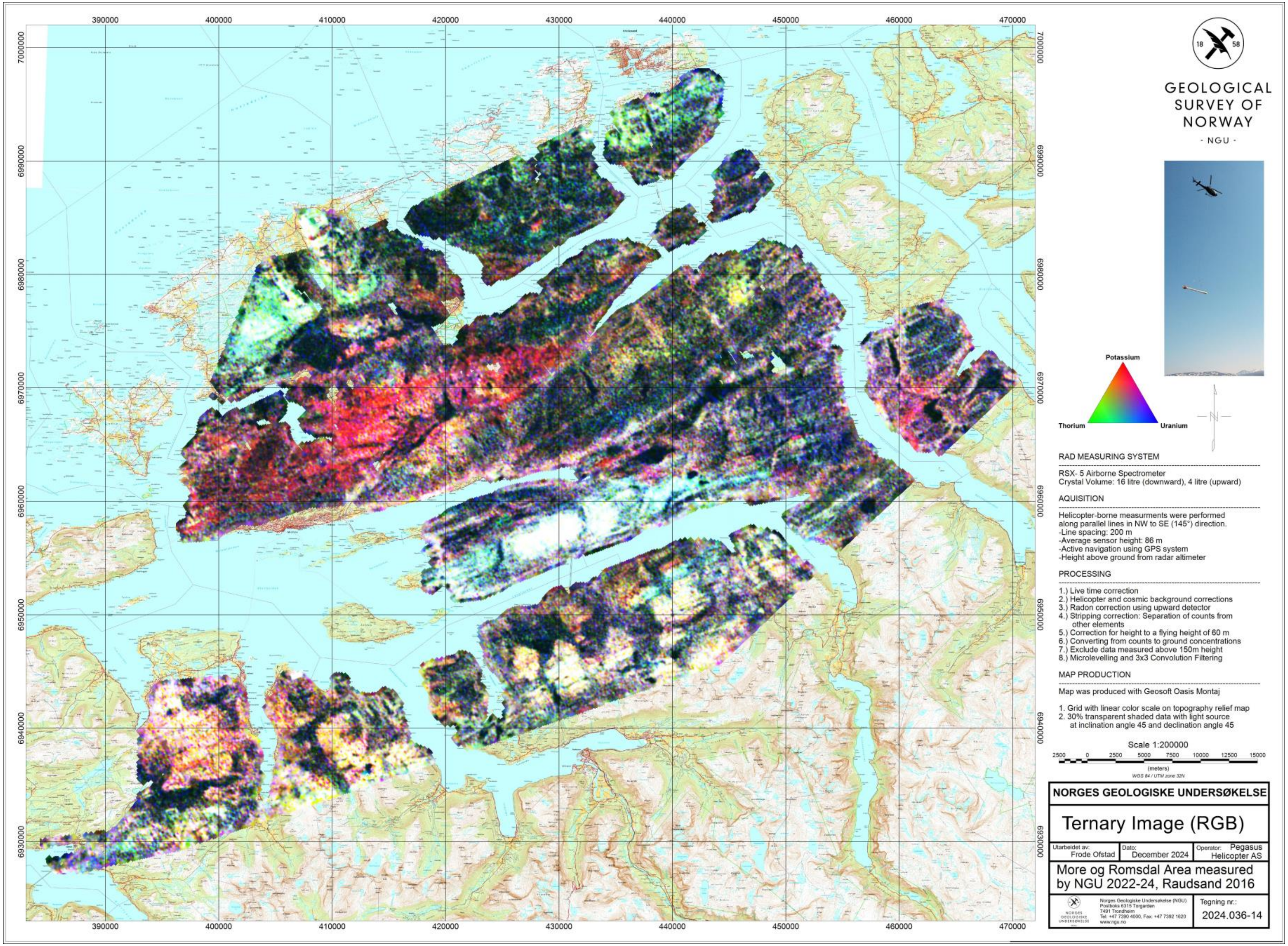

Figure 18: Radiometric Ternary Image.

GEOLOGICAL
SURVEY OF
NORWAY
- NGU -

Geological Survey of Norway
PO Box 6315, Sluppen
N-7491 Trondheim, Norway

Visitor address
Leiv Eirikssons vei 39
7040 Trondheim

Tel (+ 47) 73 90 40 00
E-mail ngu@ngu.no
Web www.ngu.no/en-gb/